NASA DEVELOP National Program
California – JPL
Summer 2020

Alaska Transportation & Infrastructure

Identifying Permafrost Subsidence Using NASA Earth Observations to Pinpoint Road and Infrastructure Vulnerability in Fairbanks, Alaska

DEVELOP Technical Report
Final Draft – August 6th, 2020

Patrick Saylor (Project Lead)
Marissa Dudek
Joshua Green
Katie Lange

Advisors
Dr. Bruce Chapman, NASA Jet Propulsion Laboratory, California Institute of Technology (Science Advisor)
Benjamin Holt, NASA Jet Propulsion Laboratory, California Institute of Technology (Science Advisor)

1. Abstract

A rapidly warming Arctic has compromised the structural integrity of critical infrastructure through accelerated permafrost thaw and thermokarst development underlying these areas. Infrastructure, including roads, bridges, and airports across the state of Alaska are particularly at risk, as permafrost underlies ~85% of the state. However, monitoring the impacts of permafrost thaw on infrastructure is largely limited to *in situ* observations and frequently identified after the damage is evident. In order to assist transportation and infrastructure decision-makers in Alaska, this project identified and quantified areas of surface subsidence near critical infrastructure. Seasonal interferograms were created using Sentinel-1 C-band Synthetic Aperture Radar (SAR) and L-band Uninhabited Aerial Vehicle SAR (UAVSAR) data to identify areas experiencing surface deformation. Additionally, Light Detection and Ranging (LiDAR) datasets were used to validate select interferograms created between 2017 and 2019. Validation of subsidence detection across platforms was performed over a 7x8 sq. kilometer field site for 2017. The strongest relationship in spatial deformation is observed between Sentinel-1 and UAVSAR with a residual root mean square error of 20 mm. These results suggest that both UAVSAR and Sentinel-1 platforms are capable of detecting surface subsidence. The higher resolution of UAVSAR is better able to resolve localized subsidence features of less than 80 meters, but is limited by temporal resolution. In conjunction, UAVSAR and Sentinel-1 can provide complementary spatial and temporal resolutions for subsidence analysis in the absence of *in situ* data.

Key Terms

Alaska, permafrost, subsidence, thermokarst, infrastructure, Sentinel-1 C-SAR, UAVSAR, LiDAR

2. Introduction

2.1 Background Information

Permafrost is a dominant terrain feature in the Arctic region, shaping about a quarter of the land areas in the northern hemisphere (Strozzi et al., 2018). Permafrost is a combination of soil and rock that has been continuously frozen for two or more years. In Alaska, permafrost can extend from a few centimeters to more than 650 meters beneath the Earth's surface (National Oceanic and Atmospheric Administration [NOAA] – Pacific Marine Environmental Laboratory, 2002). This terrain feature is structurally important to the soil, as permafrost directly influences the basic geotechnical properties of the ground (Rachlewicz & Szczucinski, 2008). These surface deformation processes pose a serious threat to the structural integrity of the Arctic region's transportation and infrastructure, such as in Alaska, where permafrost underlies 85% of the state (Alaska Department of Natural Resources [ADNR], 2020). See *Figure 1* for the statewide distribution of permafrost extent.

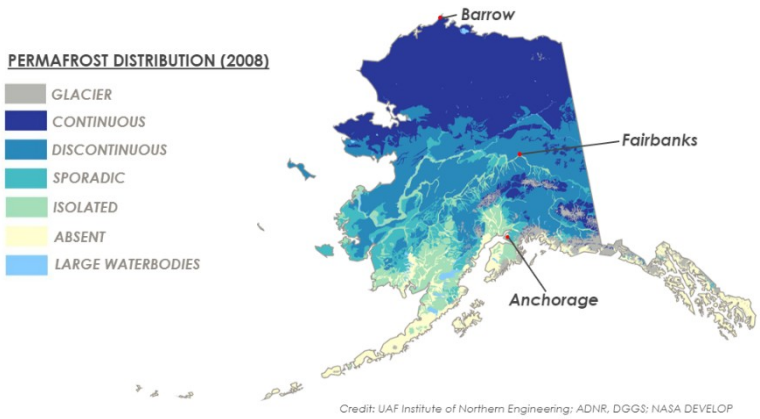

Figure 1. Map of permafrost distribution in Alaska. Permafrost is at its thickest and most extensive in the northern most part of the state and becomes thinner and more sporadic in the south. Data source: University of Alaska Fairbanks Institute of Northern Engineering, Alaska Department of Natural Resources.

Historically, surface deformation and infrastructure vulnerability from permafrost thaw have been quantified through ground-based surficial and subsurface geologic investigations (Liu et al., 2010). However, monitoring the impacts of permafrost thaw on infrastructure is limited, as *in situ* observations are expensive and time consuming to acquire. In addition, many areas affected by permafrost thaw are in remote regions or are logistically challenging to survey and frequently only identified after structural damage or failure is evident. For these reasons, monitoring surface deformation via remotely sensed data has become an attractive approach for long term and widespread comprehensive permafrost thaw identification.

The remote sensing community has addressed permafrost thaw surface deformation identification with Interferometric Synthetic Aperture Radar (InSAR), a technique used to generate a ground displacement image from a pair of SAR images. A project completed by Strozzi et al. (2018) demonstrated the feasibility of this method with Sentinel-1 C-band SAR (C-SAR) time-series interferograms to analyze summer surface displacement in the Arctic and Antarctic. They found that InSAR can be utilized to detect uniform subsidence in permafrost areas. Further comparison with L-band SAR features the best possible performance with regard to coherence over permafrost as demonstrated by Chen et al. (2012). Additional studies, such as Jones et al. (2013), have utilized repeat airborne Light Detection and Ranging (LiDAR) to detect landscape change over time and found it useful to detect and characterize thaw-related landscape changes such as thermokarst formation. In this project, the NASA DEVELOP Alaska Transportation & Infrastructure team produced permafrost deformation and thermokarst formation maps using European Space Agency (ESA) Sentinel-1 C-SAR and NASA Unmanned Air Vehicle Synthetic Aperture Radar (UAVSAR) interferograms to identify surface deformation and utilized repeat LiDAR data to validate the interferograms created.

2.2 Community Concerns

Permafrost thaw poses significant economic and environmental threats to Alaskan communities. The economic impacts can be seen in the short- and long-term structural damage of homes, buildings, roads, bridges, and oil/gas pipelines. The

environmental impacts can be felt on both local and global scales; from slope instabilities and the destabilization of critical infrastructure, to the massive release of greenhouse gases from thawing organic-rich soils (Strozzi et al., 2018). The failure of slopes can also cause an influx of sediment and permafrost melt into local waterways. *Figure 2* illustrates the impacts of permafrost thaw on communities across Alaska. Currently, the mapping of permafrost thaw and thermokarst formation is mostly limited to *in situ* data and restricts the ability of decision makers to use timely, reliable data for surface deformation identification in Alaska.

Recent increases in average global temperature trends have accelerated permafrost thaw and subsequent surface deformation in the Arctic region (Chen et al., 2012). Seasonally, the uppermost section of a permafrost layer, known as the active layer, regularly thaws and freezes. This causes the surface to sink in the summer and respectively rebound in the winter. However, when permafrost thaws more than it's able to re-freeze the surface begins to subside. This can create a positive feedback loop where surface subsidence and the formation of thermokarst features, including lakes, hummocks, and natural deforestation are increasing over time. This warming is especially pertinent in Alaska, where temperatures are increasing at twice the global average, 0.7°F every decade (Liberto, 2019).

Figure 2. Images of damage caused by permafrost deformation in Alaska. (Top Left) National Park Service, 300m long slump within the Noatak National Preserve in summer 2004. (Top Right) US Geological Survey, surface subsidence affecting spruce trees. (Bottom Left) Thomas A. Douglas, US Army Cold Regions Research and Engineering Laboratory, a roadway in Fairbanks, Alaska exhibiting buckling. (Bottom Right) Thomas A. Douglas, US Army Cold Regions Research and Engineering Laboratory, a residential home with structural damage in Fairbanks, Alaska.

2.3 Project Partners & Objectives

Partners for this project, shown in Table 1, include the US Army Corps of Engineers' Cold Regions Research and Engineering Laboratory (CRREL), the Alaska Department of Transportation & Public Facilities (ADOT&PF), the Alaska Department of Natural Resources (ADNR), and the Alaska Satellite Facility (ASF). CRREL's Fairbanks, AK office operates the Permafrost Tunnel Research Facility and desires more information about permafrost deformation within the area to ensure safety within the tunnel. ADOT&PF's decision-making entails assessing permafrost deformation near major transportation routes, infrastructure, and public facilities. Depending on the situation, ADOT&PF must decide whether to preserve or purposely thaw permafrost. ADNR is interested in the effects of permafrost on long-term groundwater quality and availability to Alaskans, as well as permafrost melt causing slope movements and drunken trees, where ground instability disrupts the vertical orientation of trees, forcing them to lean and increasing their likelihood of uprooting. Currently, partners make their decisions based on a combination of ground-based surveys and satellite imagery.

Table 1
Partner organizations for the project

Partner Organization	**Point of Contact**	**Partner Role**
US Army Corps of Engineers, Cold Regions Research and Engineering Laboratory	Tom Douglas, Senior Scientist; Christopher Hiemstra, Research Scientist	End-User
Alaska Department of Transportation & Public Facilities	Garrett Speeter, Regional Engineering Geologist	End-User
Alaska Department of Natural Resources	Ronald Daanen, Field Hydrologist	End-User
Alaska Satellite Facility	Franz Meyer, Chief Scientist	Collaborator

In order to assist partner decision making in Alaska, the objectives of this project were to use NASA Earth observations to detect permafrost subsidence and thermokarst formation, as well as to evaluate the ability and accuracy of using InSAR to pinpoint road and infrastructure vulnerability within areas of deformation. These products include a standard operating procedure of our methodology, as well as maps of seasonal and annual deformation analysis of areas surrounding critical infrastructure. A second main objective of this project was to create a Python module to automate data processing and analysis for future permafrost deformation analysis. Partners are able to use the final products of this project to inform local decision makers with concerns to permafrost thaw and thermokarst formation near areas of critical infrastructure and will be able to build capacity to continue using InSAR in future analyses.

2.4 Study Area & Period

The study area of this project was the areas surrounding the city of Fairbanks, Alaska. Fairbanks is the most populous city in the interior of Alaska, and the Fairbanks North Star Borough is the second largest metropolitan area after Anchorage (Department of Labor and Workforce Development, 2018). Project partners designated areas of interest (AOIs) in and around Fairbanks, Alaska for deformation analysis (*Figure 2)*. These areas included sections of several major

roadways designated by the ADOT&PF (approximately 80 miles in total), the CRREL Permafrost Research Tunnel, a National Ecological Observatory Network (NEON) field site, along with several isolated landslides, thermokarst, and debris lobes designated by the ADNR. The study period for this project was between January 2017 to September 2019, focusing on seasonal and annual changes in permafrost deformation.

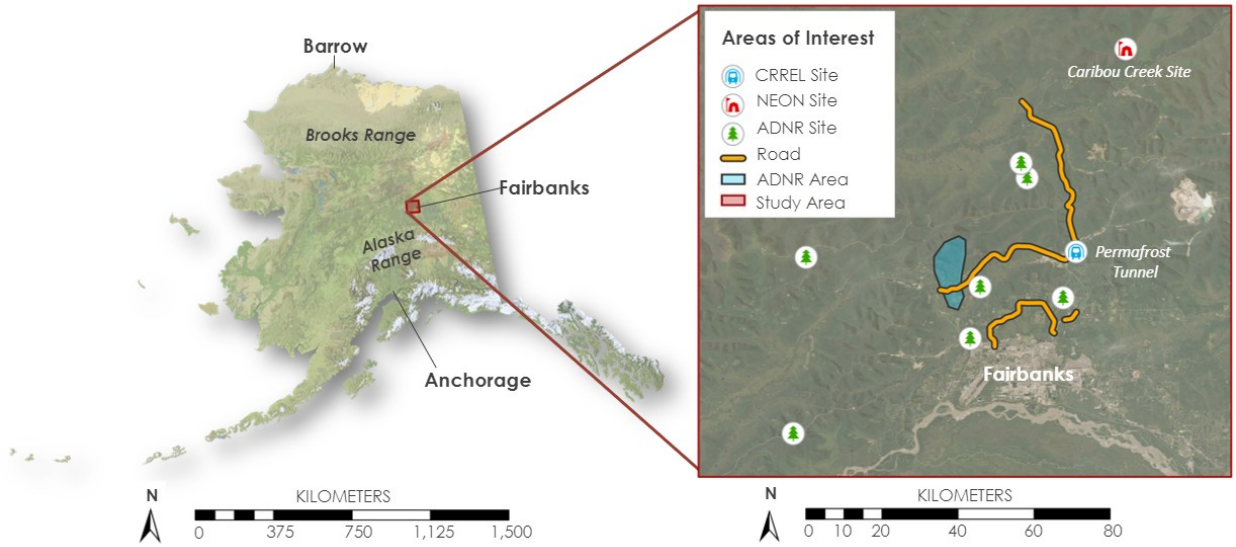

Figure 2. Map of the study area showing Fairbanks, AK and the AOIs identified by the partners, including portions of Elliot and Steese Highway, Goldstream Road, Farmer's Loop Road, the Caribou Creek NEON field site, the CRREL Permafrost Research Tunnel, and eight locations identified by ADNR including a degrading ice wedge at the CRREL AOI. Basemap image credit (right): Esri, Airbus DS, USGS, NGA, NASA, CGIAR, N Robinson, NCEAS, NLS, OS, NMA, Geodatastylerelsen, Rijkswaterstaat, GSA, Geoland, FEMA, Intermap and the GIS user community.

3. Methodology

3.1 Data Acquisition

Satellite and airborne datasets used in this project were acquired through a variety of platforms (Table 2). Sentinel-1 C-SAR Level-1 Single Look Complex (SLC) product granules were identified through the Vertex platform and accessed through the ASF Hybrid Pluggable Processing Pipeline (HyP3) tool. Sentinel-1 granules used in this project had an interferometric wide (IW) swath with vertical transmit and vertical receive (VV) polarization. The NASA Gulfstream III UAVSAR ground projection products used in this project included horizontal transmit and horizontal receive (HH) interferograms, unwrapped phase, coherence, and digital elevation models (DEMs) directly downloaded from NASA Jet Propulsion Laboratory UAVSAR data portal. The Uninhibited Aerial Vehicle (UAV) LiDAR data, providing coverage of the NEON field sites, were downloaded from the NEON data portal. The UAV LiDAR CRREL data coverage was sent to the team via online file transfer from the CRREL project partners. Additionally, the Fairbanks QL1 and QL2 2017 UAV LiDAR data were directly downloaded from the Alaska Data Elevation Portal. Lastly, the Alaska route centerlines, route mileposts, and public airport ArcMap shapefiles were acquired through the ADOT&PF Transportation

Geographic Information Section (TGIS). Project partners also provided the team with a spreadsheet of AOIs with corresponding latitude and longitude coordinates for points, start and end route mileposts for lines, and polygons for large regions.

Table 2
List of satellite and airborne datasets used in this project

Platform or Sensor	Data Product	Dates	Acquisition Method
Sentinel-1 C-SAR	Level-1 SLC, IW beam, VV polarization	Jan. 2017 to Sept. 2018	ASF Vertex
Gulfstream III UAVSAR	HH Ground Range: Coherence, Interferogram, Unwrapped phase, and DEM	Jan. 2017 to Sept. 2019	NASA Jet Propulsion Laboratory
Airborne/UAV LiDAR	NEON Field Sites 2017, 2018, and 2019 DEM	July 2017 to Aug. 2019	NSF - NEON
Airborne/UAV LiDAR	CRREL Sites 2014 and 2016 DEM	Aug. 2014 and May 2016	CRREL
Airborne/UAV LiDAR	Fairbanks QL1 & QL2 2017 DSM and DTM	May to Sep. 2017	ADOT&PF – Department of Geological and Geophysical Surveys

3.2 Data Processing

After raw data files were acquired from their respective databases, they were individually run through pre-processing steps to unify file formatting and ensure data quality. Once pre-processed, each dataset was further processed for a cross-platform deformation analysis. These steps are discussed in detail below.

A shapefile of all partner designated AOIs was created in ArcGIS Pro v2.6. Latitude and longitude coordinates were used to create point features for individual AOI locations. Polylines were created by linking milepost markers from the Alaska Mileposts and Route Centerline shapefiles from the ADOT&PF TGIS database. Polygons were used to represent local AOIs designated by the ADNR. Additionally, a 1.5 km buffer was created for each point, polyline, and polygon to encompass the surrounding terrain near AOIs. This buffer size was designated to provide a localized topographic and environmental context when analyzing deformation near these structures. The points, polylines, polygons, and buffers were then imported to an AOI geodatabase.

3.2.1 Sentinel-1 C-SAR

In this project, we utilized InSAR GAMMA processing in HyP3 to create unwrapped interferograms. Here, the ingested granule pair was spatially co-registered, computed into an interferogram, processed for topographic phase removal, processed for adaptive and multi-look phase filtering, phase unwrapped, and ultimately terrain geo-coded.

The unwrapped interferograms were then pre-processed in OpenSARLab. OpenSARLab is a Jupyter Hub based environment provided to the team by the ASF for further Sentinel-1 processing. In OpenSARLab, the unwrapped interferograms and corresponding coherence and amplitude files were downloaded and cropped to selected AOIs. Additionally, the unwrapped interferograms were culled based on timeframe and orbital characteristics, reprojected to a uniform World Geodetic System (WGS) 84 Universal Transverse Mercator (UTM) zone 6N, and atmospherically corrected using the Toolbox for Reducing Atmospheric InSAR Noise (TRAIN).

Following pre-processing in OpenSARLab, a time series analysis of the unwrapped interferograms was completed using the Generic InSAR Analysis Toolbox (GIAnT). This processing step employed the Small Baseline Subset (SBAS) analysis technique to quantity deformation over time. After running GIAnT, the deformation map outputs were converted to geotiffs for comparison with LiDAR and UAVSAR deformation change maps.

3.2.2 UAVSAR

Data processing was performed for UAVSAR through a combination of internal processing at NASA's Jet Propulsion Laboratory (JPL) and through locally run Python processing scripts. Multi-polar InSAR image pairs or granules were pre-processed by staff at NASA's JPL UAVSAR Lab. InSAR unwrapped phase diagrams, wrapped phase interferograms, and coherence products were made available and accessed through JPL's UAVSAR data portal as ASCII binary raster data in the form of Ground Range Multi-look (.GRD) files. A series of Python scripts were used to create ENVI header (.HRD) files and create a symbolic file link to produce image (.IMG) files. Additional Python scripts converted these images into georeferenced rasters in a Tagged Image File Format (TIFF).

The creation of UAVSAR deformation products involved processing of the raw unwrapped phase products in the following steps: general data cleaning, georectification, removal of NoData values, shifting of data distribution to zero, and raster calculation to determine the estimated Line of Sight (LOS) surface deformation. Deformation product statistics were calculated in QGIS and Python. As a final step prior to comparison with Sentinel-1 and LiDAR datasets, the UAVSAR deformation product was resampled and co-registered to a common coverage area and resolution for analysis.

Co-located granules with different collection dates were selected for processing as pairs to generate phase-differencing plots. These difference plots were then converted from a phase-difference to vertical displacement difference, and referenced to a standard DEM. This processed DEM and the relative change were then compared to LiDAR and Sentinel-1 datasets for analysis. It is noted that there were plans to complete a local standardization or zeroing of UAVSAR deformation products; however, this was not achieved due to time constraints. As a result, UAVSAR deformation maps serve more as qualitative or visual understandings of surface deformation.

3.2.3 LiDAR

Digital Terrain Models (DTMs) produced from LiDAR Point Clouds data were obtained for several government and research organization data portals including the US Geological Survey (USGS) 3D National Elevation Program (3DEP), the National Science Foundation National Ecological Observatory Network (NSF NEON), the US Army Corp of Engineers CRREL, and the NASA Arctic Boreal and Vulnerability Experiment (ABoVE). It is noted that the DTM products obtained from each of these sources have been previously hydro-flattened to create water features behavior as expected in a topographic map. DTM raster datasets were spatially co-registered or georectified where needed, and then mosaiced to produce a single merged raster over the entire study extent. Elevation change maps were produced through the differencing of both seasonal and annual repeat coverage DTM raster mosaics. Time series analyses were completed using these seasonal and annual elevation change maps. Spatial resolution and raster cell size were additionally rescaled to allow for direct comparison and validation of Sentinel-1 and UAVSAR datasets.

3.2.4 Cross-Platform Validation

This project is based upon a two-fold approach to investigate the response of land surface deformation to warming conditions across Alaska through remotely sensed observations and validate the performance of this data using previously established datasets. Cross-platform comparison of the sensors' deformation detection capabilities was conducted over the Caribou Creek Study Area, associated with the NSF NEON field station (*Figure 3*). This location was selected as our validation site due to consistent repeat temporal coverage across UAVSAR, Sentinel-1, and LiDAR datasets. The temporal period for comparison was spring to fall 2017, to capture the 2017 seasonal deformation period (*Figure 4*).

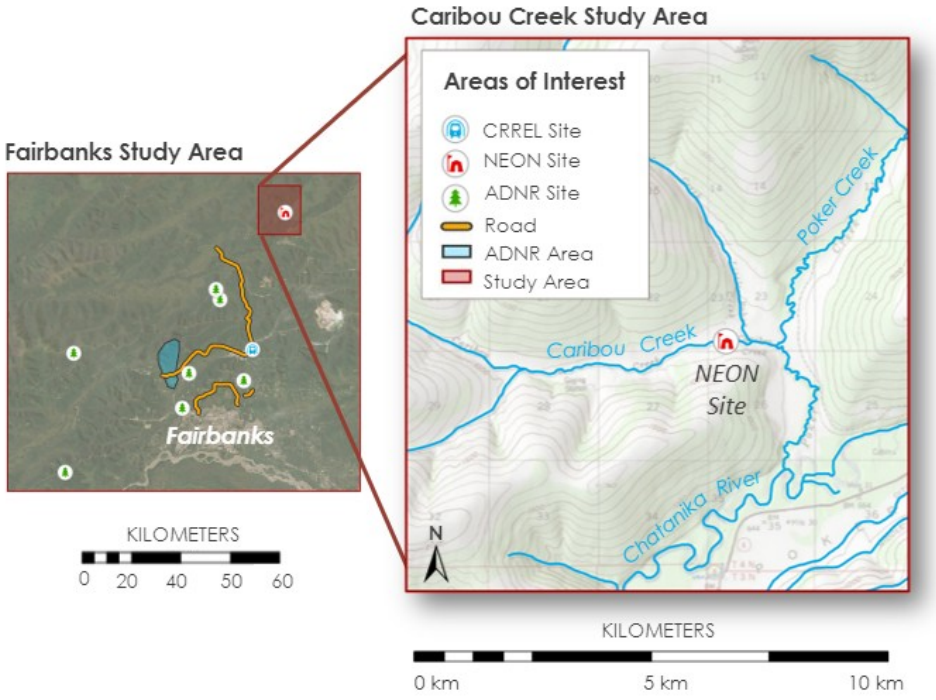

Figure 3. Caribou Creek Study Area used in cross-platform comparisons.

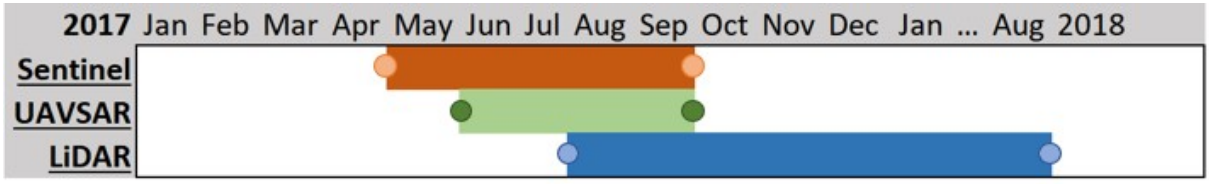

Figure 4. Sensor temporal periods for cross-platform validation analysis at Caribou Creek.

In the absence of *in situ* ground control points, the processing methodology for performing the cross-platform comparison was based on LiDAR as the validation "ground-truth" dataset. LiDAR data provides the highest spatial resolution, at approximately 1-meter coverage, as compared to lower spatial resolution UAVSAR and Sentinel-1 datasets, at 6m and 80m resolution, respectively. Pairwise comparisons between all three datasets (Sentinel-1 vs. UAVSAR, Sentinel-1 vs. LiDAR, and UAVSAR vs. LiDAR) were performed at the resolution of the coarser dataset. After resolutions had been properly matched, the root mean square error (RMSE) was computed as a pixel-by-pixel statistical comparison. The RMSE quantifies the amount of relative deformation detected in each dataset when compared to each other.

Several Python functions incorporated into the PerMA module were used to reproject, clip, and resample the data. Processing was completed in WGS84 UTM Zone 6N to ensure an equal-area projection to reduce error propagation due to transformations that might result in raster co-registration issues. To minimize error propagation in all steps of resampling the fine data, the following steps were taken to minimize error propagation in geospatial referencing: 1) Files were individually reprojected into WGS 84 UTM Zone 6N, 2) Source and target resolution files were clipped to the same extent in their original resolution. Along boundaries, "all-touched' pixels were selected, including all boundary pixels partially intersecting with the boundary extent. By clipping the same extent with all-inclusive pixel boundaries, we assume that data extents within each dataset are representative of one another, and 3) Resampling was conducted by averaging all pixels within the extent size of an individual cell of the coarser raster. To enforce pixel co-registration, the transformation function prioritizes raster length and width geometry over explicit pixel size dimensions (*Figure 4*). This allows the transformation to preserve shape for one-to-one comparison. It should be noted that the application of this transform method requires post-facto analysis to determine that pixel sizes are appropriately matched at the desired resolution. No boundary effects were incorporated in the clipping or resampling. NoData values were excluded from all calculations.

Finally, "difference in difference" comparisons were conducted to evaluate the z-scores of each dataset within the Caribou Creek Study Area domain. For each comparison pair, the (originally) higher resolution dataset was subtracted from the (originally) lower resolution dataset to generate consistent figures for comparison (*Figure 5 and Appendix B*).

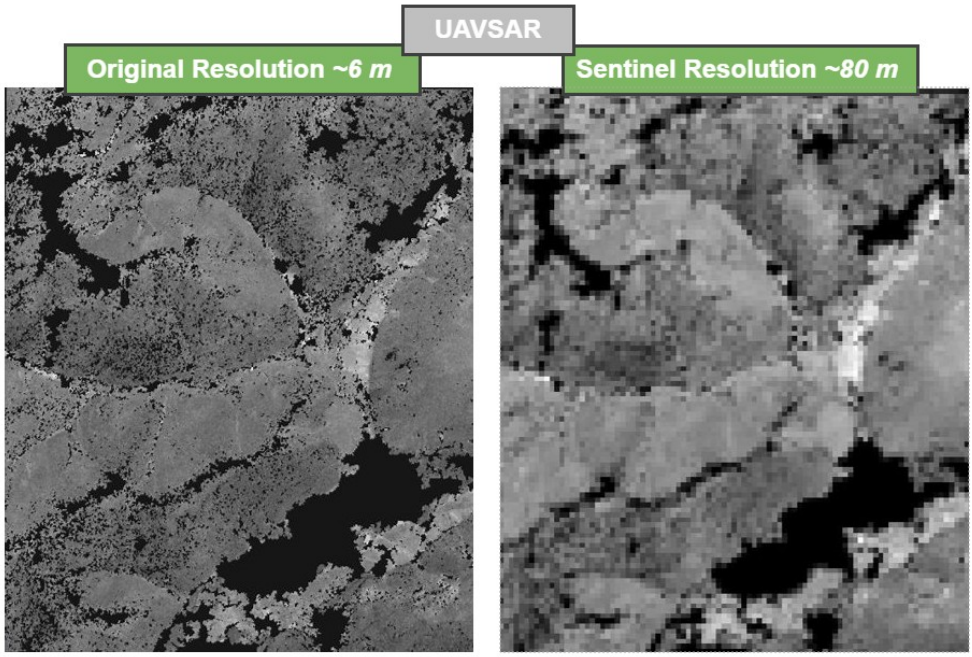

Figure 4. Example of UAVSAR data clipped to the Caribou Creek Study Area, at original (6m) and Sentinel-1 (80m) resolution. Note that spatial features, geometry, and extent are preserved during the rescaling of spatial resolution.

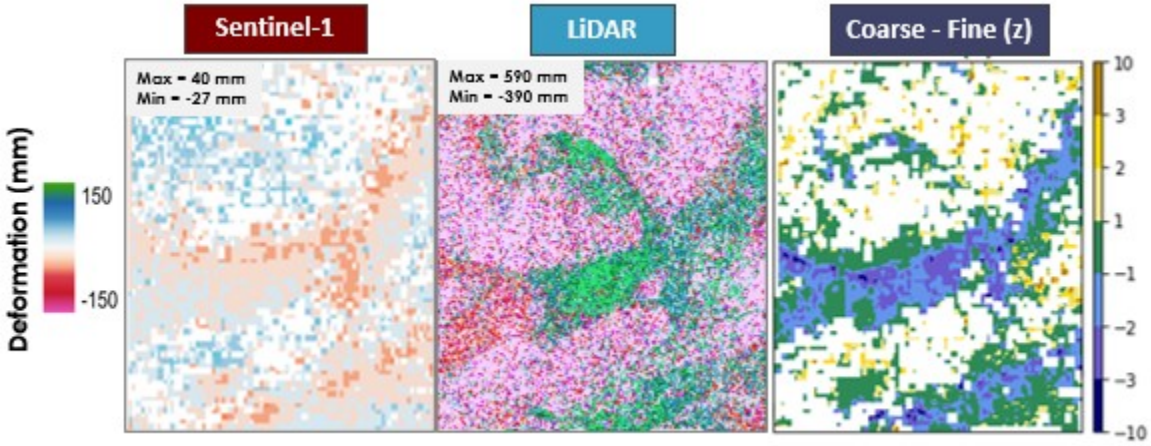

Figure 5. Sentinel and LiDAR relative difference analysis at the Caribou Creek validation site. The LiDAR data were resampled to match Sentinel-1 spatial resolution for comparison. Both LiDAR and Sentinel-1 deformation values were converted to a z-score to complete the relative difference analysis. The extreme values, in both the negative and positive directions, indicate areas with diverging agreement across sensors. Alternately, the green areas, or z-score values ranging from 1 to –1, indicate areas of agreement across sensors.

In order to avoid complications with horizontal displacement assumptions required to convert UAVSAR data to vertical displacement, each dataset was converted to a z-score. This allows the relative deformation at each pixel, relative to the dataset domain to be represented, creating a like unit of comparison across datasets with differing units. Where possible, analyses were completed in vertical displacement (millimeters).

4. Results & Discussion

4.1 Analysis of Results

Results in the following section will be presented first as cross-platform validation comparisons and then individually as stand-alone deformation analyses. Our validation analysis is focused solely on the Caribou Creek NEON field site. This area was selected to allow for the greatest overlap in spatial and repeat temporal coverage across all sensors. The cross-platform validation results at Caribou Creek are shown in *Figure 6*. The seasonal deformation z-score differenced images illustrate the relative differences between Sentinel-1 and LiDAR, Sentinel-1 and UAVSAR, and LiDAR and UAVSAR. Although analysis is conducted at Sentinel-1 spatial resolution to maintain consistency, each image depicts the finer resolution z-score subtracted from the coarser resolution z-score. The extreme values, in both the negative and positive directions, indicate areas with diverging agreement across sensors. Alternately, the green areas, or z-score values ranging from 1 to –1, indicate areas of agreement across sensors. Visual inspection of all three images broadly suggest agreement across areas known to be relatively flat, with inconsistent signatures detected over more complex terrain.

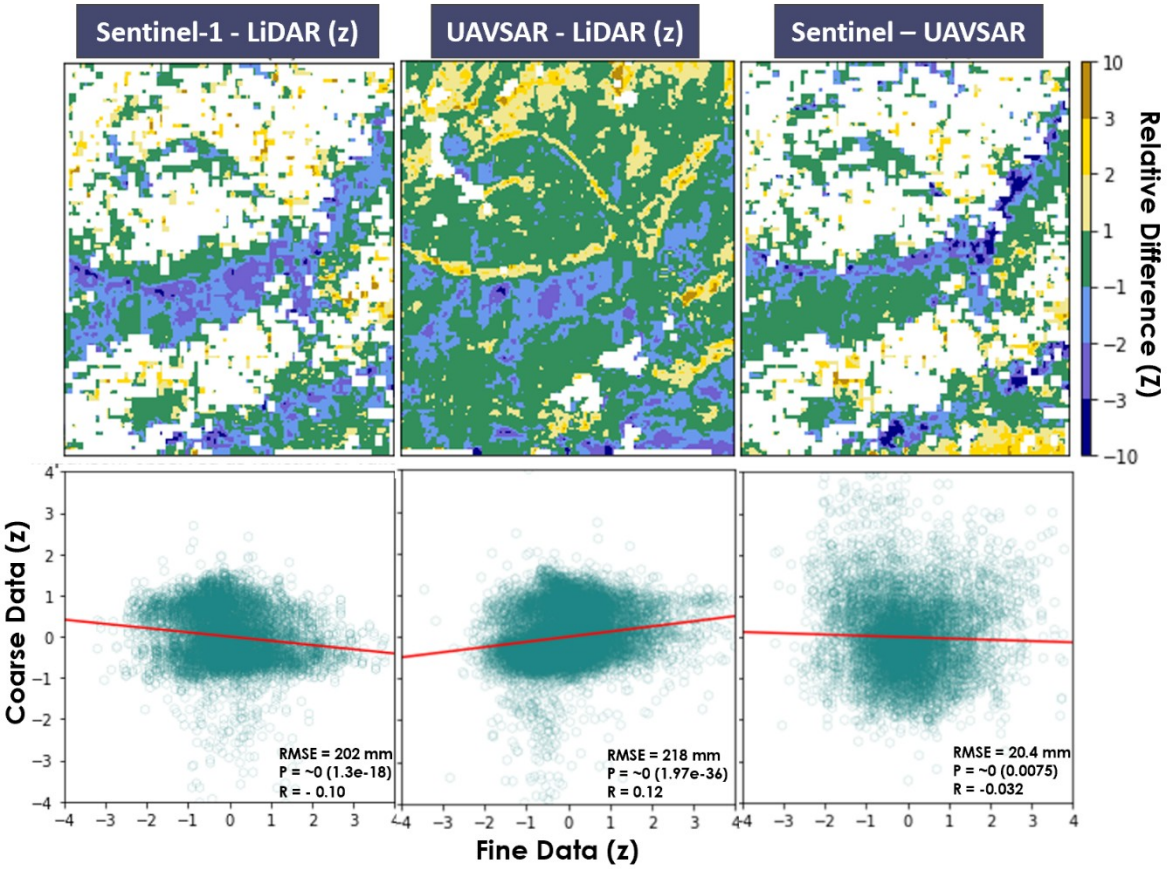

Figure 6. Top: Seasonal deformation z-score differences show the relative differences between datasets. Value extremes represent areas where the datasets diverge in agreement, and green areas represent good agreement between the datasets. Bottom: One-to-one pixel comparisons in each dataset are displayed. To maintain consistency, originally 'coarse' resolution datasets are located on the horizontal axis and

‘fine’ on the vertical axis. Values displayed are the z-scored values over the domain for each dataset.

Additionally, the pixel comparison graphs show a high degree of variability and do not indicate a strong linear relationship across any platforms, suggesting weak relationships between areas observed to be deforming across each dataset (*Figure 6*). However, in conjunction with the seasonal deformation z-score differenced images, the pixel comparison graphs suggest the lack of a linear relationship may be a result of a signal to noise issue, where areas of strong diverging trends exist in close proportion to areas in agreement in the graphs.

The strongest relationship in spatial deformation is observed between Sentinel-1 and UAVSAR, quantified in *Table 3.* The Sentinel-1 and UAVSAR RMSE was 20 mm which suggests general spatial agreement between the Sentinel-1 and UAVSAR, in comparison to the higher RMSE between Sentinel-1 and LiDAR and UAVSAR and LiDAR. Qualitatively, the spatial differencing relationships at the Caribou Creek validation site suggest general agreement. This is likely a reflection of the general spatial agreement in all datasets of areas of relative local deformation. This implies that all three platforms, with different limitations, produce some degree of spatial internal consistency.

Table 3
Cross-platform pairwise linear regression statistics

	Sentinel-LiDAR	**UAVSAR-LiDAR**	**Sentinel-UAVSAR**
RMSE (mm)	202	218	20
R-value	-0.10	0.12	-0.03
P-value	~0	~0	~0

In *Figure 7*, we show the UAVSAR and Sentinel-1 seasonal deformation results at Farmers Loop. The UAVSAR and Sentinel-1 maps were placed on a common color scale for comparison. The SAR image ranges from -50 to 50 mm of deformation while UAVSAR ranges from -150 to 150 mm of deformation. These images provide a look into the relative deformation for each sensor. Visually, the Sentinel-1 and UAVSAR seasonal deformation analysis at Farmers Loop show spatial agreement below mile markers 1, 2, 6, 7, and 8. Alternatively, they display diverging results on the northern side of the road. Additional seasonal and annual deformation maps of AOIs can be found in Appendix A.

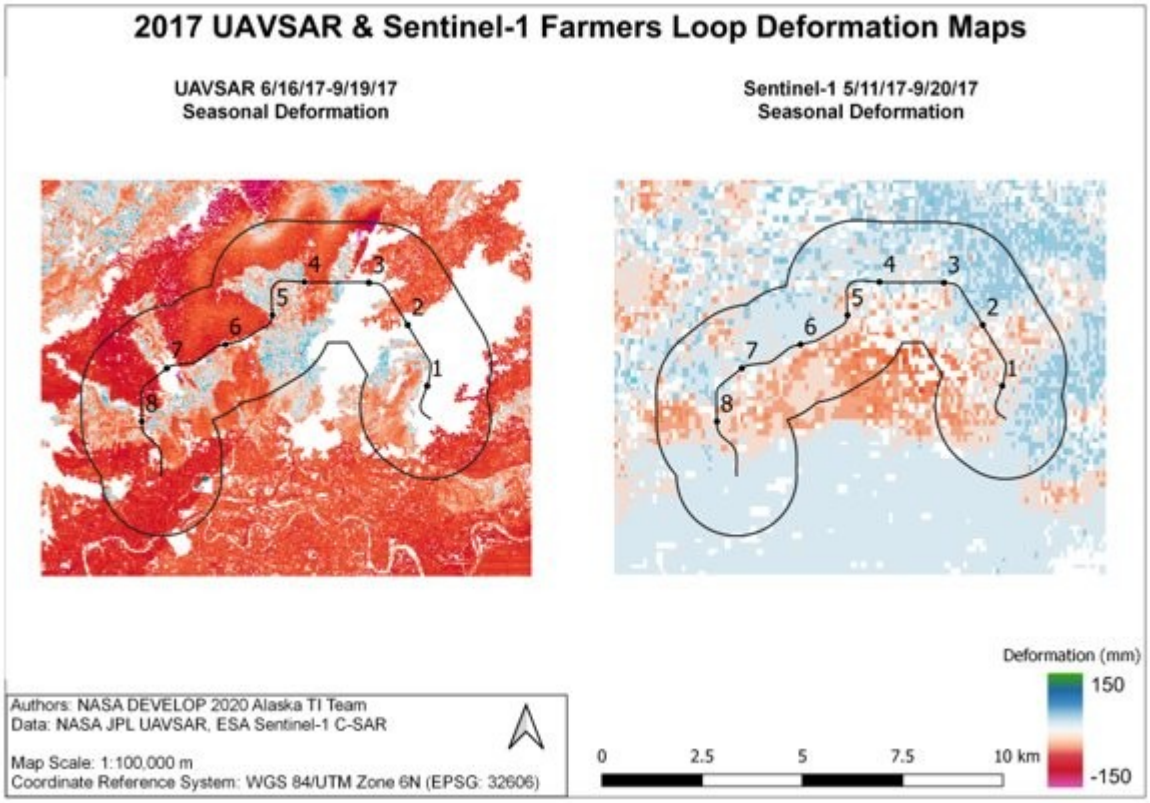

Figure 7. 2017 Seasonal deformation at Farmers Loop from both UAVSAR and Sentinel-1. Z-score differences show the relative differences between datasets. The UAVSAR and Sentinel-1 maps were placed on a common color scale for comparison. The SAR image ranges from -50 to 50 mm of deformation while UAVSAR ranges from -150 to 150 mm of deformation.

4.2 Limitations & Future Work

This project was partially limited due to temporally and spatially sparse repeat coverage of LiDAR, and partially due to data quality issues with LiDAR datasets selected for validation. The NEON 2018 LiDAR data was corrupted in external collection/processing where half of the available coverage measured an artificial additional meter of elevation. This portion of the LiDAR 2018 dataset was excluded from our analysis. Our validation area was reduced due to this limitation. This project was also limited due to upscaling UAVSAR and LiDAR to match Sentinel-1 resolution. Pixel values were grouped and averaged in this method; however, this step was necessary to validate across platforms. This project encountered an error in the 2018/2019 UAVSAR swath where there was a long-range tilt error. Additionally, coherence issues were observed in UAVSAR data over water features and forested land.

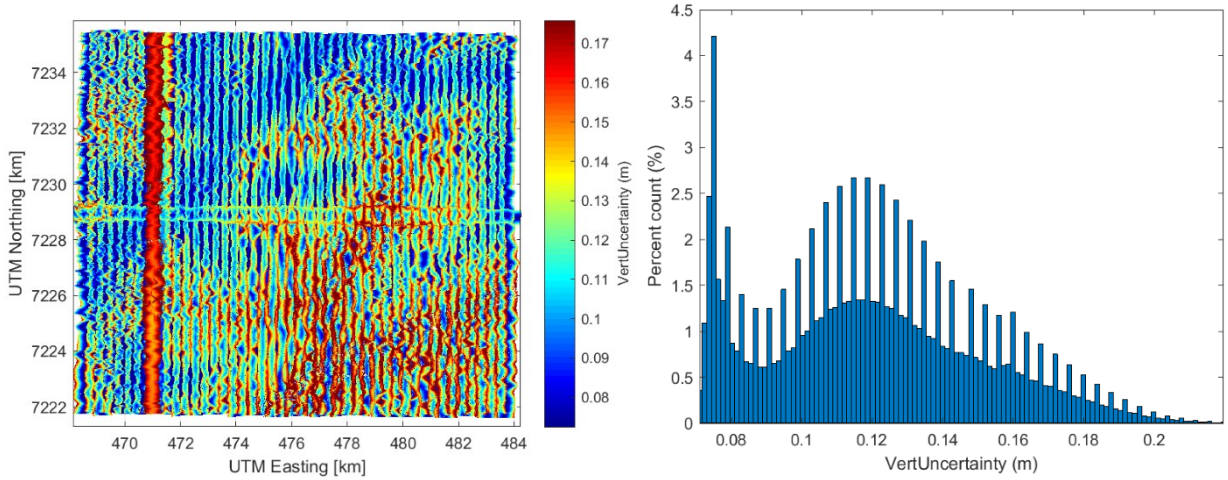

Figure 8. LiDAR uncertainty over the Caribou Creek Study Area collected in 2018 indicates a degree of vertical uncertainty that may negatively impact results in cross-comparison analyses. Here, flight path artifacts are observed to influence a substantial portion of the data, of greater than 15 centimeters in some cases. Left and Right figure: (Goulden, 2018)

Throughout this project, we found the methodology that had been developed can be expanded upon in four main factors. First, the project can be expanded upon by extending the study area to AOIs designated by the partners outside of the Fairbanks region (*Figure 9*). These AOIs include several major roadways and bridges, the Noorvik and Shageluk Airports, as well as known locations of thermokarst lake expansion, unstable slopes, and debris lobes. Second, by further comparing new and repeat LiDAR to UAVSAR and Sentinel-1, the validity and accuracy of ground-truthing surface elevation fluctuation overtime using LiDAR can be further investigated. Third, the automated Permafrost Measurement and Analysis (PerMA) python module developed in this project could be expanded upon in several ways; automating data acquisition from intra-organizational datasets, pre-processing of UAVSAR to correct for line-of-sight long-range tilt acquired during data collection, and by detecting a consistent baseline for cross-platform relative deformation analysis. Finally, the methodology can be improved upon by investigating the effect that the underlying geology and soil have on seasonal and annual permafrost thaw.

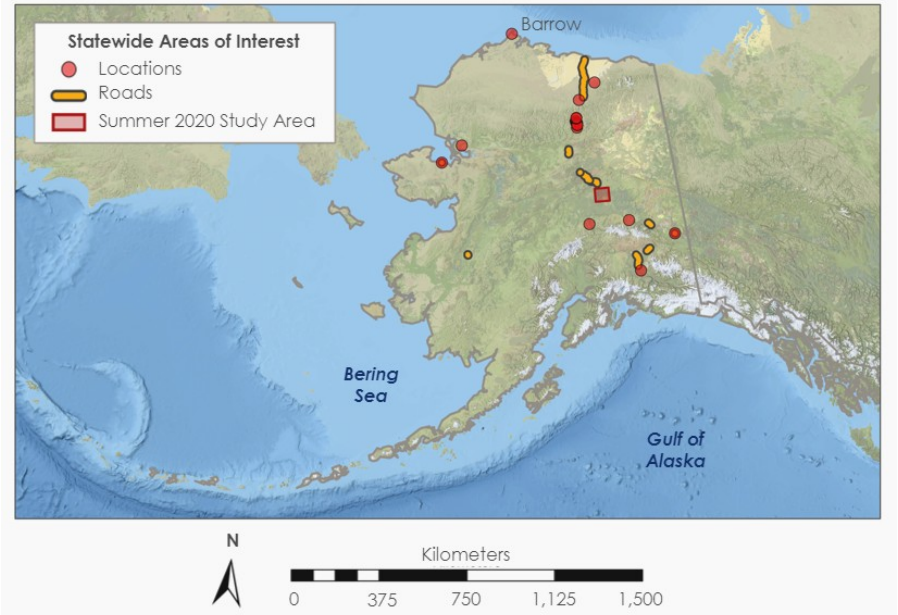

Figure 9. Alaska statewide areas of interest designated by the Summer 2020 project partners.

5. Conclusions

We found that the independent implementation of InSAR data is useful in the evaluation of surface subsidence due to permafrost thaw and thermokarst formation in the absence of *in situ* data. However, further work is required to substantiate the linkage between the deformation detected by these sensors and its subsequent impact on critical infrastructure. Preliminary results from this analysis suggest that both localized and broad-scale deformation in the proximity of critical infrastructure can be identified. However, the end-goals of the user must be evaluated to properly pair needs with the data most suitable for the job. Sentinel-1 observations allow for broad temporally consistent analyses at low resolution, whereas UAVSAR analysis is useful in the identification of localized features, though largely limited by flight path spatial coverage and temporal data availability. Project partners can use the findings of this project to prioritize their needs in identifying the appropriate tools for identifying areas of deformation. Further, the software advances provided through the PerMA python module, developed over the course of this project, will assist partners in the pre-processing, processing, and data analysis of these remotely sensed data platforms in the future.

6. Acknowledgments

We thank everyone at the California – JPL DEVELOP node for their support and guidance during this term and for providing the Earth observation data required for this project.

Dr. Bruce Chapman (NASA Jet Propulsion Laboratory, California Institute of Technology)
Ben Holt (NASA Jet Propulsion Laboratory, California Institute of Technology)
Cecil Byles (NASA DEVELOP National Program, Lead/Fellow)

A special thanks to our project partners who provided us with areas of interest, remotely sensed data, and their expertise throughout this project.

Dr. Tom Douglas (US Army Corps of Engineers, Cold Regions Research and Engineering Laboratory)
Dr. Chris Hiemstra (US Army Corps of Engineers, Cold Regions Research and Engineering Laboratory)
Garrett Speeter (Alaska Department of Transportation & Public Facilities)
Dr. Ronald Daanen (Alaska Department of Natural Resources)
Dr. Franz Meyer (Alaska Satellite Facility)

Additionally, a thank you goes to Alex Lewandowski and Soumitra Sakhalkar with the Alaska Satellite Facility and the University of Anchorage respectively for their guidance in the use of OpenSARLab and HyP3.

This material contains modified Copernicus Sentinel data (2017-2019), processed by ESA.

Any opinions, findings, and conclusions or recommendations expressed in this material are those of the author(s) and do not necessarily reflect the views of the National Aeronautics and Space Administration.

This material is based upon work supported by NASA through contract NNL16AA05C.

7. Glossary

ADNR - Alaska Department of Natural Resources
ADOT&PF - Alaska Department of Transportation & Public Facilities
AOI - Area of Interest (e.g. road section, field site, landslide, thermokarst, etc.)
ASF - Alaska Satellite Facility
CRREL - US Army Corps of Engineers, Cold Regions Research and Engineering Laboratory
DEM - Digital Elevation Model
Earth observations - Satellites and sensors that collect information about the Earth's physical, chemical, and biological systems over space and time
GIAnT - Generic InSAR Analysis Toolbox
LiDAR - Light Detection and Ranging, a remote sensing method that uses pulsed laser light to measure distance to ground surface elevation
NEON - National Ecological Observatory Network
OpenSARLab - A cloud-based service for SAR analysis operated by the Alaska Satellite Facility
Permafrost - Ground that remains completely frozen for at least two straight years
Subsidence - Sinking of ground surface elevation either suddenly or gradually
SAR - Synthetic Aperture Radar, a remote sensing method that uses C-band radar
Thermokarst - Irregularly textured surface with pits, lakes, and karstic features formed as permafrost and ice thaws in the Arctic region
UAVSAR - Uninhabited Aerial Vehicle Synthetic Aperture Radar

8. References

Alaska Department of Natural Resources Geological & Geophysical Surveys. (2020). *Permafrost & Periglacial Hazards*. (2020). Retrieved from https://dggs.alaska.gov/hazards/permafrost.html

Chen, F., Lin, H., Li, Z., Chen, Q., & Zhou, J. (2012). Interaction between permafrost and infrastructure along the Qinghai-Tibet Railway detected via jointly analysis of C- and L-band small baseline SAR interferometry. *Remote Sensing of Environment, 123*, *523-540.* https://doi.org/10.3390/rs10020298

Department of Labor and Workforce Development. Department of Labor and Workforce Development, State of Alaska. (2018). *Department Alaska Population Estimates by Borough, Census Area, and Economic Region*. Retrieved from https://live.laborstats.alaska.gov/pop/

Goulden, T. (2018). *L3 discrete lidar processing and QA information for 2017 BONA.* In Neon AOP QA report. Received from: http://data.neonscience.org

Jones B., Stoker J., Gibbs A., Grosse G., Romanovsky V., Douglas T., Kinsman N., & Richmond B. (2013). Quantifying landscape change in an arctic coastal lowland using repeat airborne LiDAR. *Environmental Research Letters, 8 (4)*. http://dx.doi.org/10.1088/1748-9326/8/4/045025

Liberto, Tom Di. (2019, July 16). *High Temperatures Smash All-Time Records in Alaska in Early July 2019*. NOAA Climate. www.climate.gov/news-features/event-tracker/high-temperatures-smash-all-time-records-alaska-early-july-2019.

Liu L., Zhang T., & Wahr J. (2010). InSAR measurements of surface deformation over permafrost on the North Slope of Alaska. *Journal of Geophysical Research,115.* https://doi.org/10.1029/2009JF001547

NOAA Pacific Marine Environmental Laboratory. (2002, December 10). *Land-Permafrost*. Arctic Change. https://www.pmel.noaa.gov/arctic-zone/detect/land-permafrost.shtml

Rachlewicz R. & Szczucinski W. (2008). Changes in thermal structure of permafrost active layer in a dry polar climate, Petuniabukta, Svalbard. *Polish Polar Research, 29*(3). Retrieved from https://www.researchgate.net/publication/236845394_Changes_in_thermal_structure_of_permafrost_active_layer_in_a_dry_polar_climate_Petuniabukta_Svalbard

Strozzi, T., Antonova, S., Gunther, F., Matzler, E., Vieira, G., Wegmuller, U., Westermann, S., & Bartsch, A. (2018). Sentinel-1 SAR Interferometry for surface deformation monitoring in low-land permafrost areas. *Remote Sensing, 10*(9). https://doi.org/10.3390/rs10091360

9. Appendices

Appendix A
Area of Interest Deformation Analysis

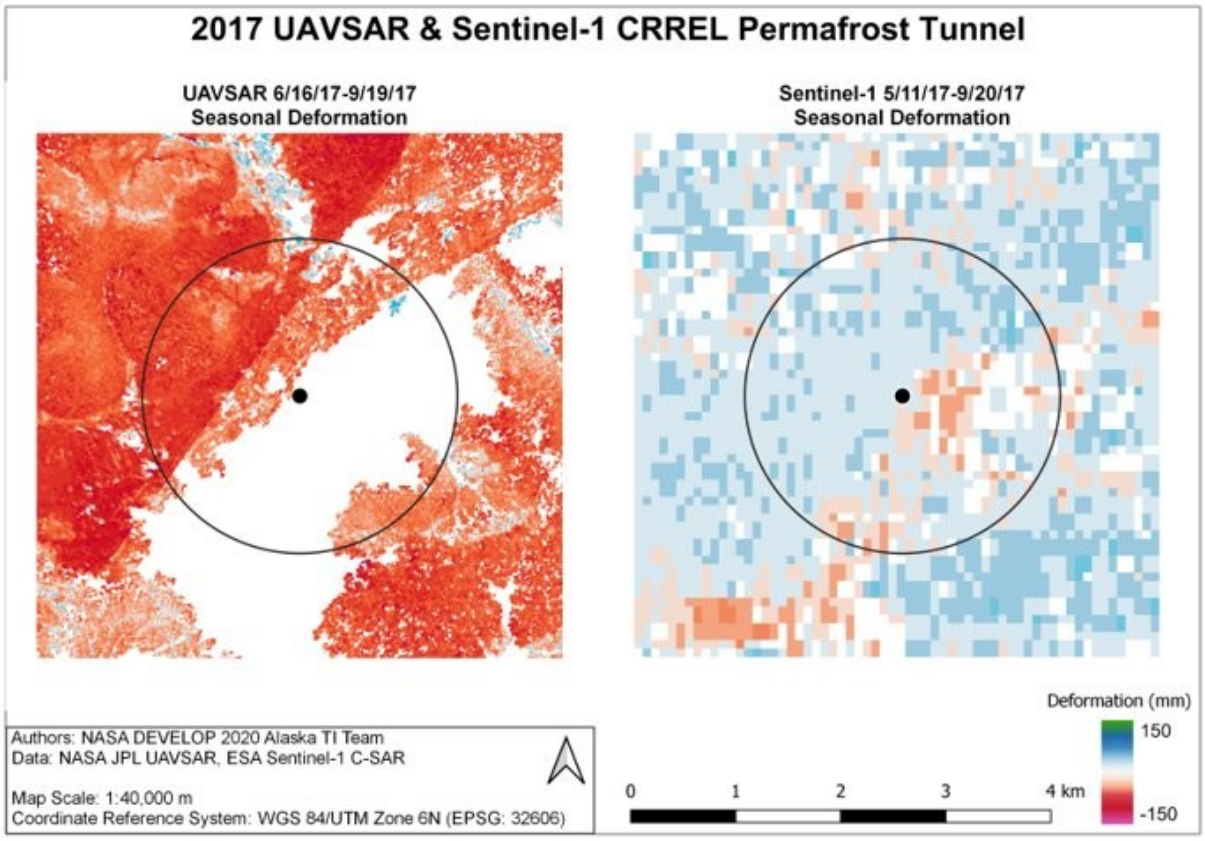

Figure A1. UAVSAR and Sentinel-1 seasonal 2017 deformation at CRREL Permafrost Research Tunnel. The two datasets were placed on a common scale for comparison. UAVSAR deformation ranges from +/- 150 mm of deformation while Sentinel-1 deformation ranges from +/- 50 mm of deformation. In the UAVSAR image, there is significant NoData in the southeast region of the tunnel. This is attributed due to a phase unwrapping error as a result of low coherence. This decorrelated data could be attributed to flooding, forests, or extreme deformation.

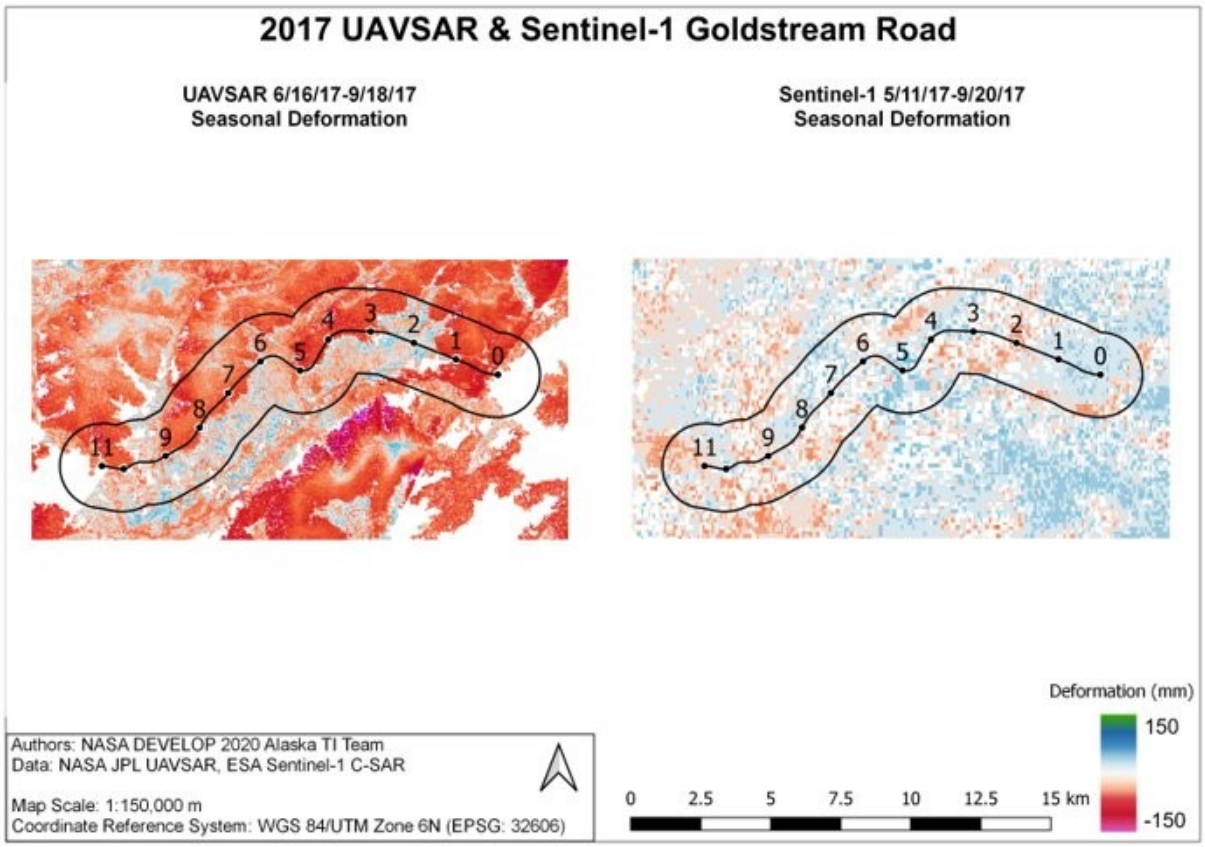

Figure A2. UAVSAR and Sentinel-1 seasonal 2017 deformation at Goldstream Road. The two datasets were placed on a common scale for comparison. UAVSAR deformation ranges from +/- 150 mm of deformation while Sentinel-1 deformation ranges from +/- 50 mm of deformation. The images should be analyzed as relative deformation rather than absolute deformation. UAVSAR and Sentinel-1 show some spatial consistency beneath mile makers 2, 3, and 4 with deformation occurring south of Goldstream Road.

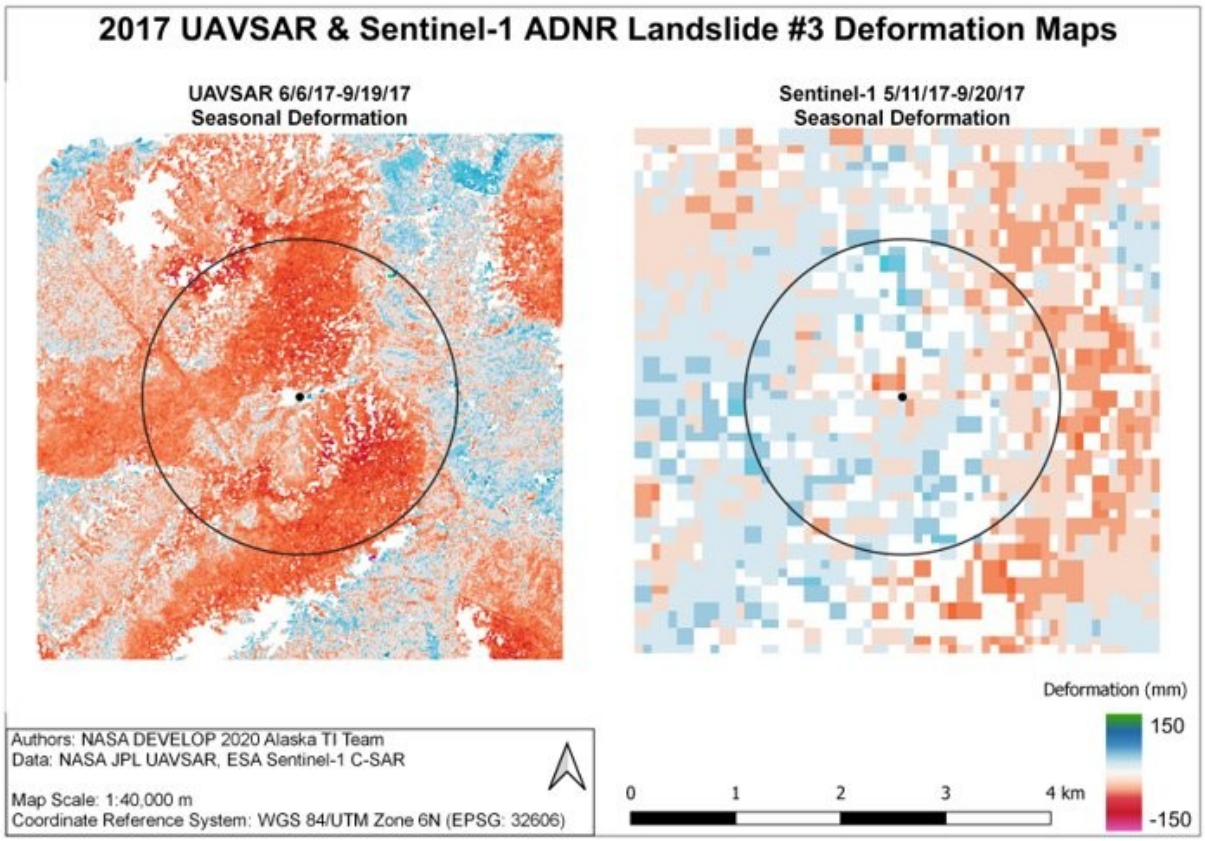

Figure A3. UAVSAR and Sentinel-1 seasonal 2017 deformation maps at Alaska Department of Transportation Landslide 3 selected area of interest. The two datasets were placed on a common scale for comparison. UAVSAR deformation ranges from +/- 150 mm of deformation while Sentinel-1 deformation ranges from +/- 50 mm of deformation. The images should be analyzed as relative deformation rather than absolute deformation. UAVSAR and Sentinel-1 show some spatial agreement in the images; however, they show deformation on varying scales. Future studies could improve the spatial agreement by selecting a standard “0 point” in both images.

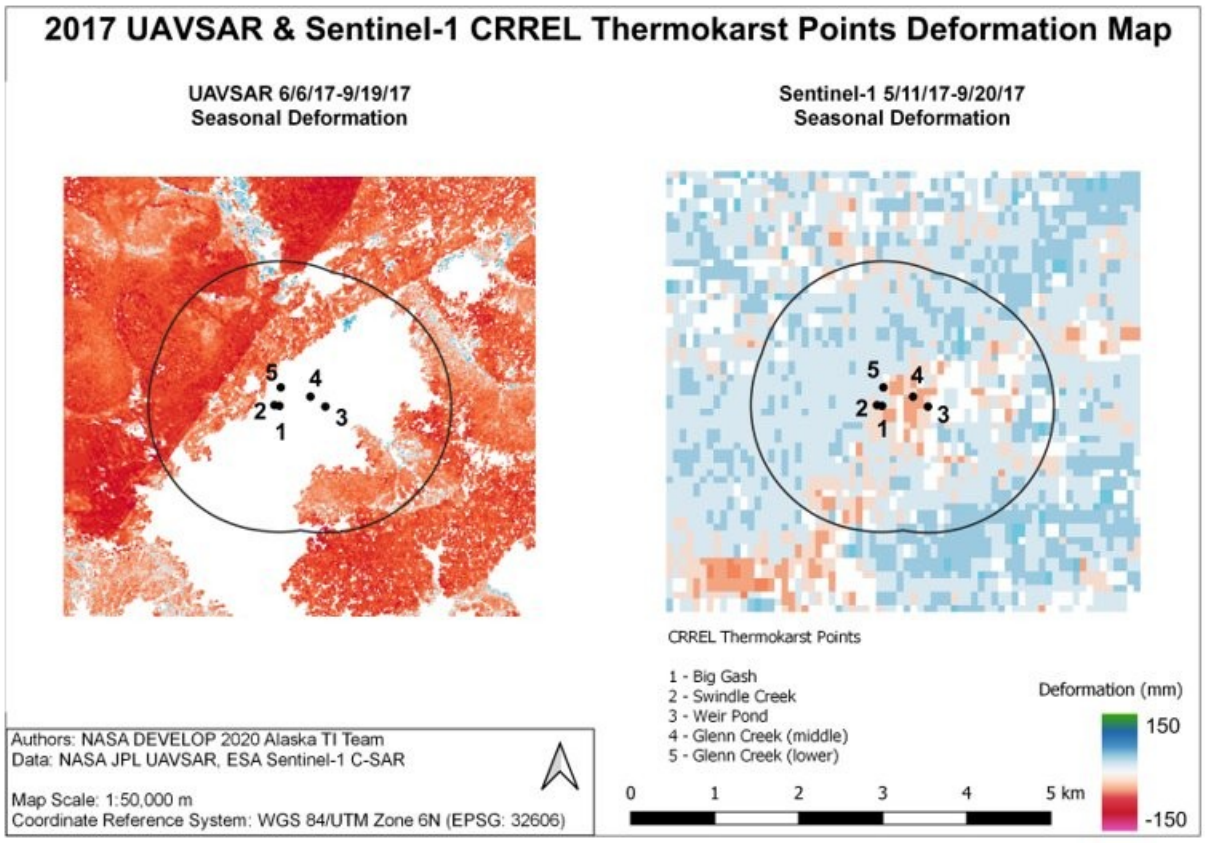

Figure A4. UAVSAR and Sentinel-1 seasonal 2017 deformation maps at five thermokarst locations designated by CRREL. The two datasets were placed on a common scale for comparison. UAVSAR deformation ranges from +/- 150 mm of deformation while Sentinel-1 deformation ranges from +/- 50 mm of deformation. The images should be analyzed as relative deformation rather than absolute deformation. In the UAVSAR image, there is significant NoData in the southeast region of the buffer. This is attributed due to a phase unwrapping error as a result of low coherence. This decorrelated data could be attributed to flooding, forests, or extreme deformation. However, the Sentinel-1 deformation map detects surface subsidence in the area surrounding the thermokarst points.

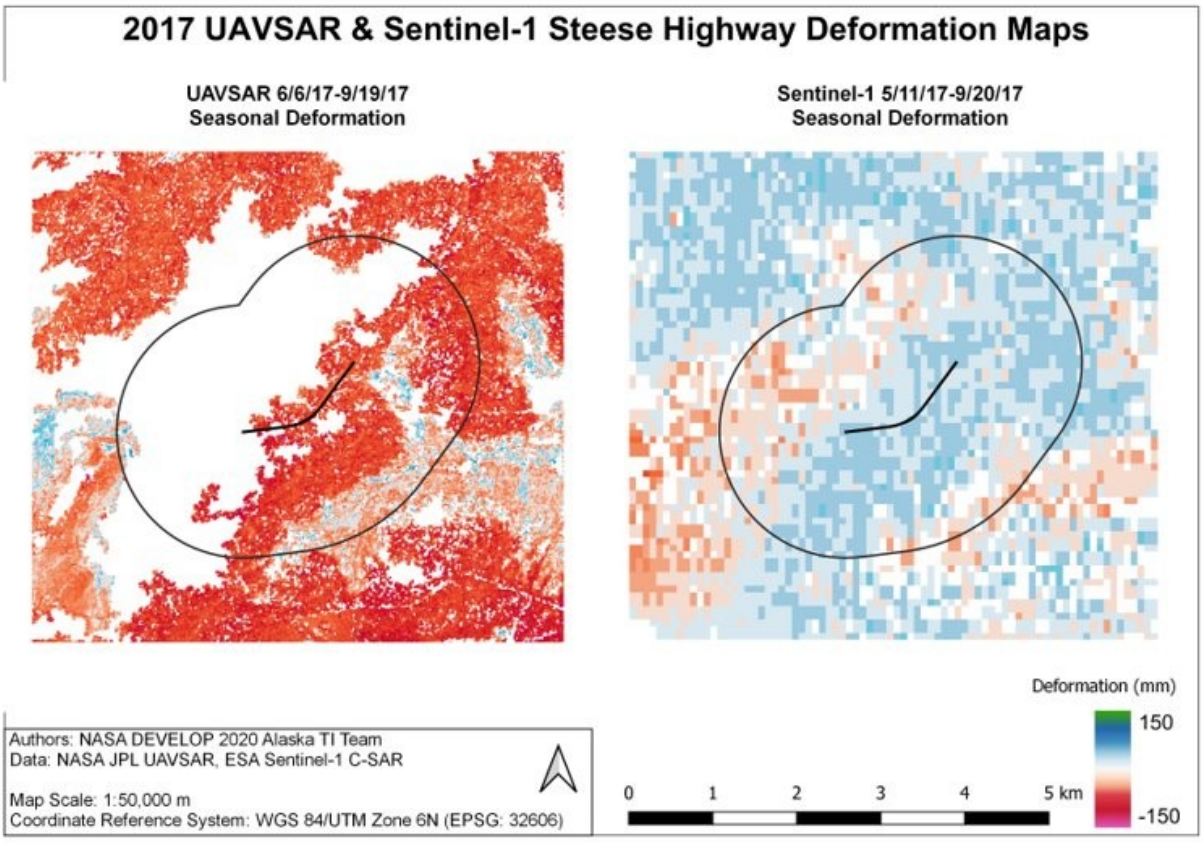

Figure A5. UAVSAR and Sentinel-1 seasonal 2017 deformation maps at Steese Highway. The two datasets were placed on a common scale for comparison. UAVSAR deformation ranges from +/- 150 mm of deformation while Sentinel-1 deformation ranges from +/- 50 mm of deformation. The images should be analyzed as relative deformation rather than absolute deformation. In the UAVSAR image, there is significant NoData in the northwest region of the buffer. This is attributed due to a phase unwrapping error as a result of low coherence. This decorrelated data could be attributed to flooding, forests, or extreme deformation. However, the Sentinel-1 deformation map detects surface subsidence in the area surrounding the in the decorrelated area in the UAVSAR deformation map.

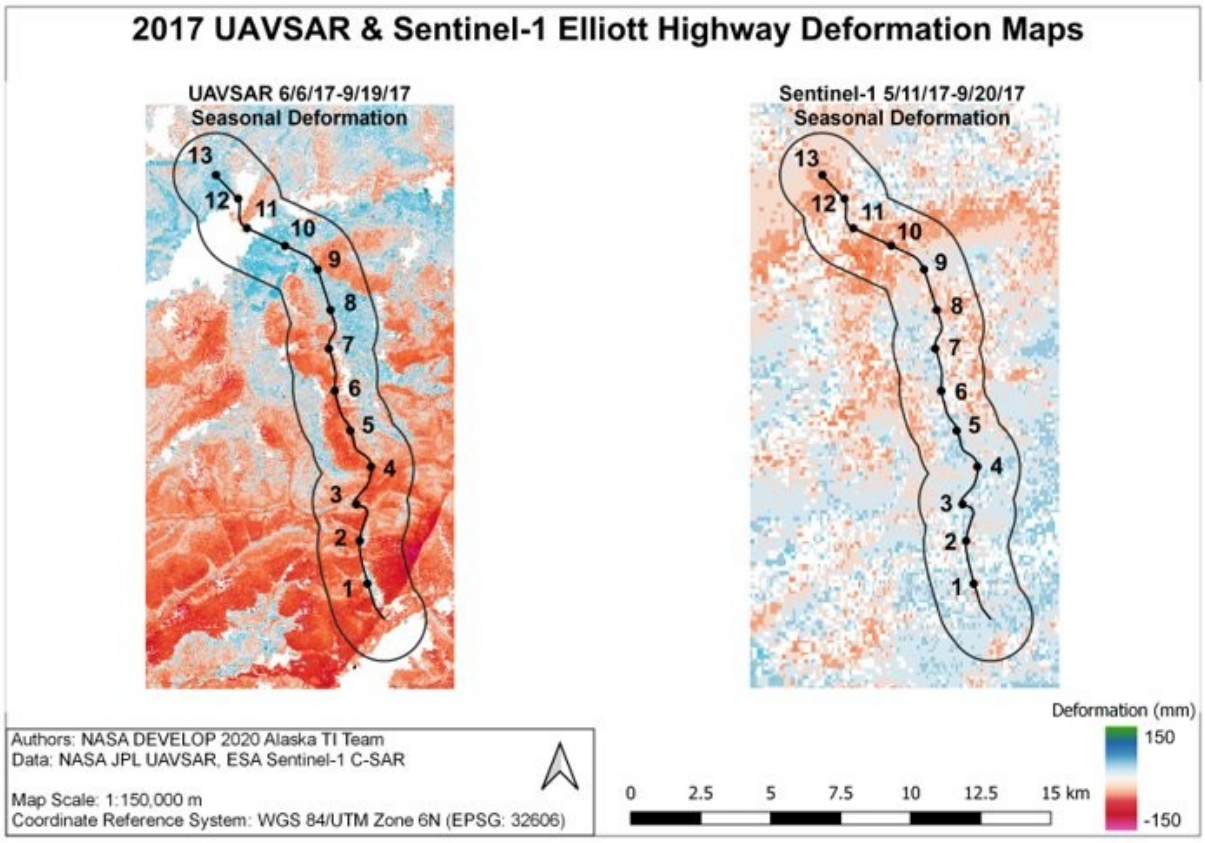

Figure A6. UAVSAR and Sentinel-1 seasonal 2017 deformation maps at Elliott Highway. The two datasets were placed on a common scale for comparison. UAVSAR deformation ranges from +/- 150 mm of deformation while Sentinel-1 deformation ranges from +/- 50 mm of deformation. The images should be analyzed as relative deformation rather than absolute deformation. The images show varying degrees of deformation. However, they illustrate similar spatial trends.

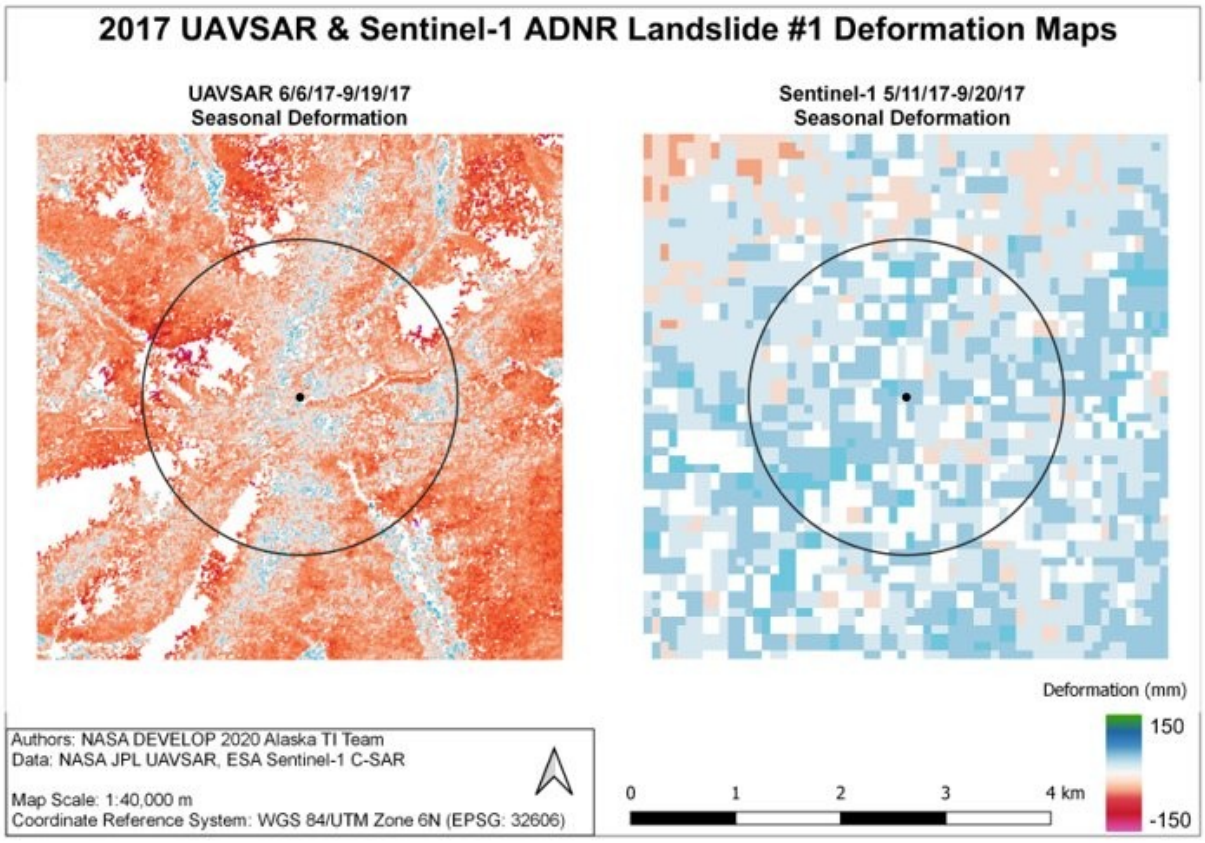

Figure A7. UAVSAR and Sentinel-1 seasonal 2017 deformation maps at the Alaska Department of Transportation Landslide 1 selected area of interest. The two datasets were placed on a common scale for comparison. UAVSAR deformation ranges from +/- 150 mm of deformation while Sentinel-1 deformation ranges from +/- 50 mm of deformation. The images should be analyzed as relative deformation rather than absolute deformation.

Appendix B
Relative Difference Analysis

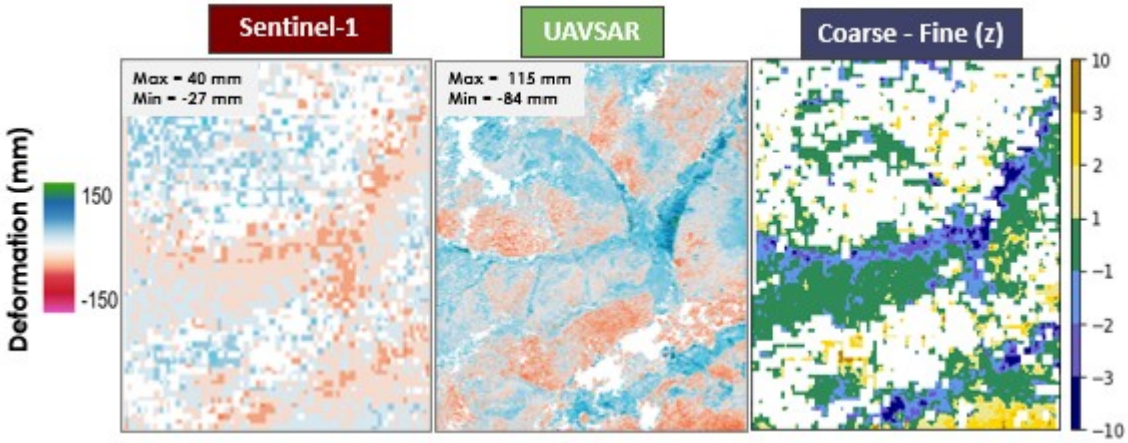

Figure B1. Sentinel and UAVSAR relative difference analysis at the Caribou Creek validation site. The UAVSAR data were resampled to match Sentinel-1 resolution for comparison. Both UAVSAR and Sentinel-1 deformation values were converted to a z-score to complete the relative difference analysis. The extreme values, in both the negative and positive directions, indicate areas with diverging agreement across sensors. Alternately, the green areas, or z-score values ranging from 1 to –1, indicate areas of agreement across sensors.

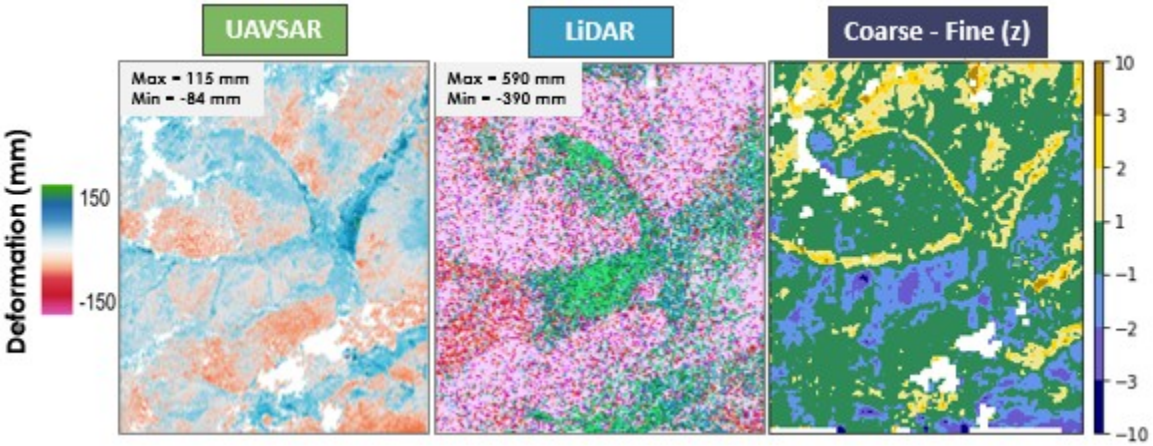

Figure B2. UAVSAR and LiDAR relative difference analysis at the Caribou Creek validation site. The LiDAR data were resampled to match UAVSAR resolution for comparison. Both LiDAR and UAVSAR deformation values were converted to a z-score to complete the relative difference analysis. The extreme values, in both the negative and positive directions, indicate areas with diverging agreement across sensors. Alternately, the green areas, or z-score values ranging from 1 to –1, indicate areas of agreement across sensors.